International Journal of Applied Earth Observation and Geoinformation 19 (2012) 12–23

Contents lists available at SciVerse ScienceDirect

International Journal of Applied Earth Observation and Geoinformation

journal homepage: www.elsevier.com/locate/jag

Estimating regional heavy metal concentrations in rice by scaling up a field-scale heavy metal assessment model

Meiling Liu[a], Xiangnan Liu[a,*], Jonathan Li[b,c], Ting Li[a]

[a] China University of Geosciences, School of Information Engineering, 29 Xueyuan Road, Beijing 100083, China
[b] Xiamen University, School of Information Science and Engineering, 422 Siming Road South, Xiamen, Fujian 361005, China
[c] University of Waterloo, Department of Geography and Environmental Management, 200 University Avenue West, Waterloo, Ontario, Canada N2L 3G1

ARTICLE INFO

Article history:
Received 7 February 2012
Accepted 24 April 2012

Keywords:
Heavy metal assessment model
Upscaling
Hyperion data
ASD data
Piecewise function

ABSTRACT

The objective of this study was to determine the levels of heavy metals cadmium (Cd) and copper (Cu) in rice by upscaling a field-scale heavy metal assessment (FHMA) model from field to regional scale. The FHMA model was established on the basis of spectral parameters in combination with soil parameters by employing a generalized dynamic fuzzy neural network. The piecewise function and ordinary kriging were developed to suit the upscaled spectral parameters and soil parameters, respectively. In addition, the network structure and fuzzy rules, which had already been developed in the FHMA model, would be subsequently extracted as those of the regional-scale heavy metal assessment (RHMA) model. The results showed that the latter performed well at prediction with a correlation coefficient (R^2) and model efficiency (ME) greater than 0.70, and can be applied to other areas, perhaps universally. This study suggests that it is feasible to accurately estimate regional heavy-metal concentrations in rice by scaling up the FHMA if such a strategy is appropriately selected and finds that the piecewise function is well suited to transferring spectral data from a field to a regional scale.

1. Introduction

Proximal sensing has proven to be useful in assessment of heavy-metal concentrations in crop under controlled laboratory conditions and field-scale trials (Font et al., 2002, 2004; Rosso et al., 2005; Zengin and Munzuroglu, 2005; Chi et al., 2009; Liu et al., 2010, 2011a). However, these field-scale approaches are often laborious and limited to small area studies (Kooistra et al., 2001, 2004; Clevers et al., 2004; Noomen et al., 2006, 2012). Regional-scale approaches using satellite data for assessing large-area heavy-metal concentrations in crop are therefore needed. The goal of this study was to build a regional model based on imagery, in order to provide regional-scale information about levels of heavy metal pollution. The heavy metal assessment model in laboratory conditions and field-scale conditions is usually generated by combining ground data and spectral data, which are derived from crop leaf or canopy reflectance. In contrast, the RHMA model is established based on pixels in remotely sensed imagery.

The importance of scale issues is widely recognized, such as in hydrology (Becker and Braun, 1999), ecology (Petrosillo et al., 2010; Pelosi et al., 2010) and social sciences (Schroder and Schmidt, 2006). Different methods have been employed to estimate systems responses across scales. Generally speaking, scaling transformations are classified into two different schemes. The first is the manipulation of model across scales. Some common methods are to adjust model parameters or structure, derive response function or response coefficients for the (often higher) scale at which the model is applied (Parry et al., 2004; Adam et al., 2011). The second is the manipulation of data at different spatial resolutions. Approaches include extrapolation and singling out, interpolation and sampling, aggregation and disaggregation (Zobeck et al., 2000; Wang et al., 2002; Ewert et al., 2011). The choice of methods depends on the specific objectives and the scales or levels considered (Zarco-Tejada et al., 2001; Volk et al., 2008).

In remote sensing, scaling methods comprise deriving empirical or physical models that establish a relationship between biophysical variables (e.g., surface temperature, evapotranspiration, leaf area index and spectral information) from satellite sensors at different scales (Hong et al., 2005, 2009; Liu et al., 2006; Martinez et al., 2009). When using remote sensing and geographic information systems (GIS), accurately scaling-up spatial data of a variable and their uncertainties from a finer to a coarser spatial resolution has been widely required in mapping and managing natural resources and ecological and environmental systems (Hong et al., 2009; Nagarajan et al., 2010). The majority of these studies focused on determining optimal spatial resolution for data collection and mapping, and on scaling-up spatial data from one scale to another. However, there has been little research on transformation of heavy metal

* Corresponding author. Tel.: +86 10 82321796; fax: +86 10 82322095.
E-mail address: liuxncugb@163.com (X. Liu).

0303-2434/$ – see front matter © 2012 Elsevier B.V. All rights reserved.
http://dx.doi.org/10.1016/j.jag.2012.04.014

assessment model from field-scale to regional-scale. The objective of this study was to establish the RHMA model to estimate regional heavy-metal concentrations in rice based on the FHMA model developed in our previous study (Liu et al., 2011b).

2. Study area and data

2.1. Study area

Two paddy fields in Changchun, Jilin Province, China (43°05′59.15″N, 125°08′26.69″E) were selected as the study Areas A and B (see Fig. 1). Area A is covered by fewer paddy fields than Area B. The study areas are about 20 km away from each other and similar with regard to climate, historical land use and soil series. The areas are within the temperate continental climate zone with a mean annual rainfall of 522–615 mm, where soils are dominated by black soils with sufficient organic matter (2–4%). Jijing 105 rice genotype (*Oryza sativa* L.) is cultivated in the study areas. The planted rice is supplied with abundant fertilizers, manures and irrigation water to avoid other environmental factors causing unwanted stress. The main physicochemical characteristics of the soil are showed in Table 1. From Table 1, the total carbon (C), total nitrogen (N), total kalium (K) and total phosphorus (P) can ensure to meet the needs of rice growing normally based on local rice management experience. Heavy metals (Zn, Pb, Cr and As) of two study areas are both lower than the background level, while Cu and Cd concentration are higher than the background level. Since the rice is not stressed by nutrient deficiency, water stress etc., and it could therefore be hypothesized that rice are mainly influenced and stressed by Cu and Cd. As such, this study focuses on predicting Cu and Cd concentration in rice. In this study, Area A was used to establish the RHMA model for estimating heavy-metal concentrations, while Area B was applied to investigate whether the RHMA model established is not used extensively in another area. In short, Area A and Area B were taken as the study area of establishment and validation of regional-scale model, respectively.

2.2. Field ground data

The field ground data sets used in this study include soil data, heavy-metal concentration data in rice and hyperspectral data collected by using an Analytical Spectral Devices (ASD) FieldSpec Pro spectrometer. The spectral data collection was carried out during four days during a typical rice growth season in 2008 and 2009, respectively, which corresponded to the seeding, tillering, booting and mature growth stages of rice. All spectral measurements were taken under cloudless or near-cloudless conditions between 10:00 and 14:00. This spectrometer was fitted with fiber optics having a 10° field of view (FOV), and was operated in the 350–2500 nm spectral regions with sampling intervals of 2 nm. Reflectance spectra were measured through calibration with a standardized white spectralon panel. A panel radiance measurement was taken before and after the crop measurement with 2 scans each time. The measurements were carried out from a height of 1 m above the rice canopy. Each site was scanned 10 times and these measurements were then averaged for the particular site. The 120–160 samples from heavy metal of rice leaves were scanned in each growth stage of rice per paddy field. Apart from abnormal spectral data, the whole set of samples was split into two subsets, namely about 2/3 for training ($n = 69$) and the rest ($n = 45$) for an external testing.

Rice and soil sampling were taken almost simultaneously with measurements of canopy spectral reflectance. The leaves per rice and soil per sample site were both collected and placed into respective sealed plastic bags to obtain biochemical composition, such as nutrient elements and heavy-metal concentrations. Heavy-metal concentrations in soil and rice were determined by an atomic absorption spectrophotometer (AAS). Total C, total N, total K were measured by elemental analyzer (Leco, USA), and

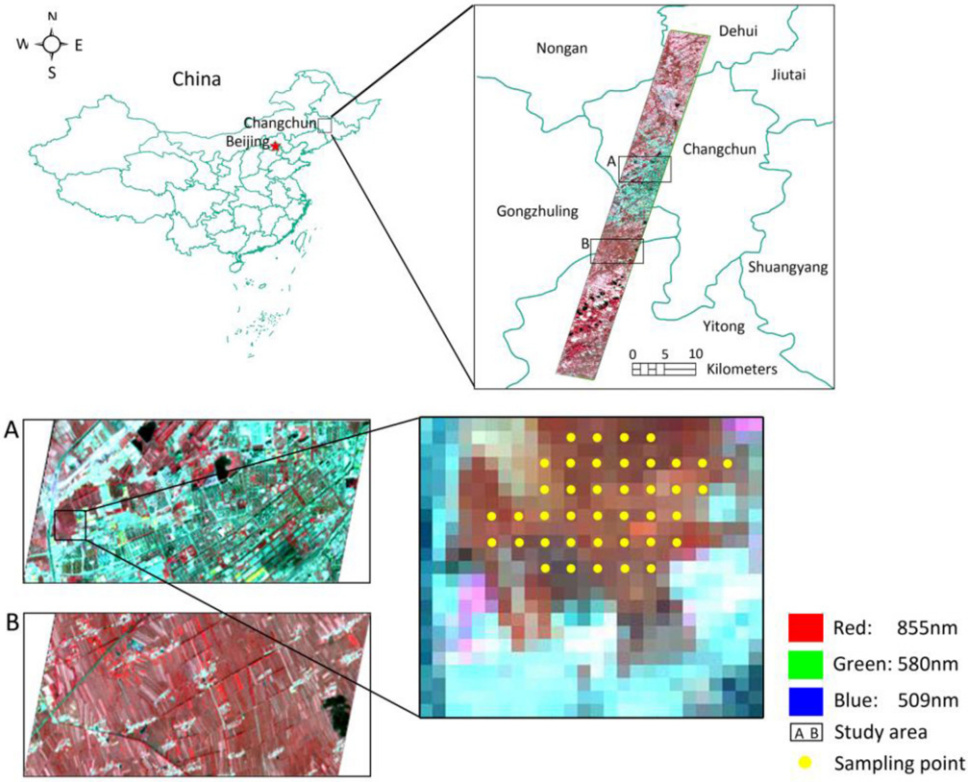

Fig. 1. The study Areas A and B in the city of Changchun, Jilin, China.

total phosphorus in the soil were determined by spectrophotometer analyzer (751GD, Shanghai Metash Instrument Co. Ltd.) at the Chinese Academy of Agricultural Sciences (Bao, 2005). In this context, soil pH was determined in a paste with a ratio of 1:2.5 soils to water using a pH meter Model PHS-3C. Soil organic matter was analyzed according to Chinese Country Reference Material/Reference Material (CRM/RM) information center.

2.3. Hyperion hyperspectral data

In this study, a scene of the NASA Earth Observing One (EO-1) satellite Hyperion image covering the city of Changchun, Jilin, China was acquired on 7 October 2009, about one week before field ground data for rice in maturity growth stage were collected, and when the paddy soil was dry. The Hyperion can provide a high resolution hyperspectral imager capable of resolving 220 spectral bands (from 0.4 to 2.5 μm) with a 30 m resolution. The EO-1 Sensor Hyperion can image a 7.5 km by 100 km land area per image, and provide detailed spectral mapping with a spectral range of 0.2–2.4 μm and a spectral resolution of 10 nm across all 220 channels with high radiometric accuracy.

3. Method

To effectively monitor heavy-metal concentrations in rice leaves on a large scale, we present a method for upscaling from field to regional scale. This method can be implemented by the following steps (see Fig. 2):

(1) Data collecting and processing, including the ASD, Hyperion hyperspectral, and soil property data.
(2) Upscaling of input parameters, for the spectral parameters, the piecewise function was adopted to achieve scale transformation, while for the soil parameters, spatial interpolation were used to complete scale transformation.
(3) Extracting of model structure, which derived from FHMA model based on a generalized dynamic fuzzy neural network (GDFNN). Such structure would be subsequently used in the RHMA model in order to predict heavy metal concentrations.

The RHMA model is established across obtaining regional-scale input variables and performing fuzzy rules and structure of FHMA model.

3.1. Preprocessing of Hyperion data

The preprocessing of Hyperion imagery includes five steps:

(1) Eliminating useless bands in Hyperion imagery, in which the signal-to-noise ratio (SNR) was too low because of the effect from atmospheric scattering and water vapor absorption (Keshava, 2001, 2003).
(2) Replacing bad lines, which are defined as some vertical lines in the image having low or no Digital Number (DN) values compared with adjacent columns. The Gray-scale Slope Threshold (GST) method was applied to automatically identifying bad lines in each band.
(3) Removing vertical strips in Hyperion imagery. The Global Normalization Method (GNM) was used for eliminating the negative effect of vertical strips (Datt et al., 2003).
(4) Atmospheric correction using the Fast Line-of-sight Atmospheric Analysis of Spectral Hypercubes (FLAASH) software tool.
(5) Geometric correction, by selecting quadratic polynomial method and cubic convolution method, the image was corrected to WGS-84 (World Geodetic System1984) coordinate

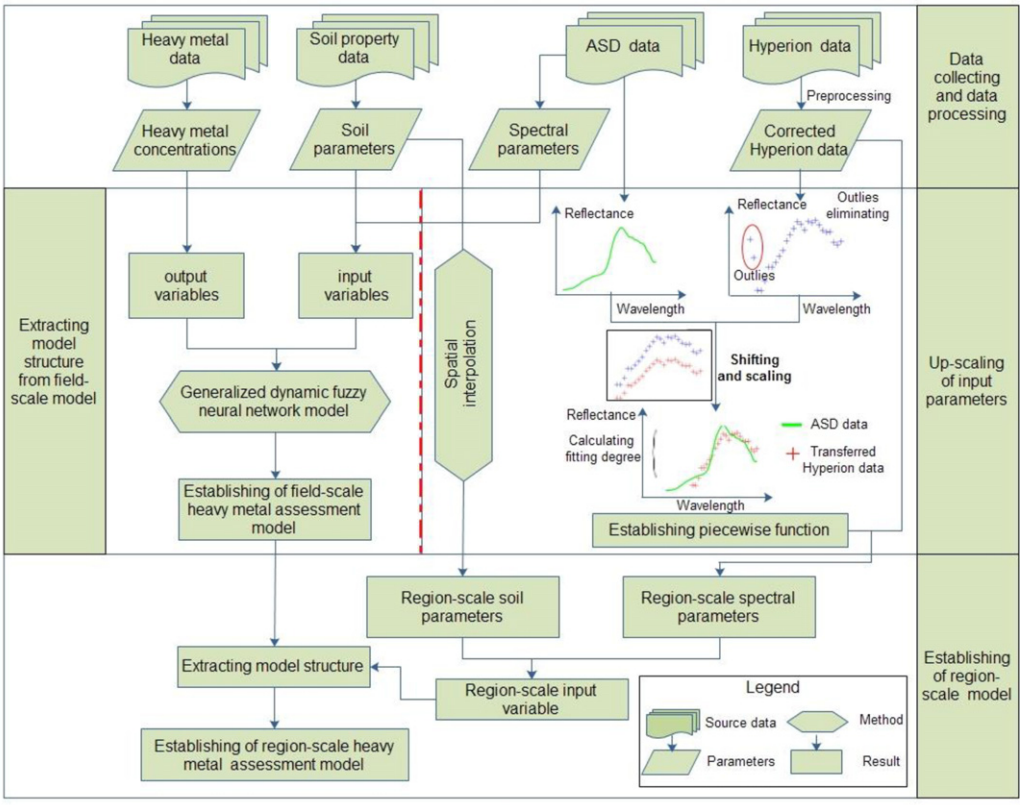

Fig. 2. Flow chart for estimating regional heavy metal concentrations in rice based on FHMA model.

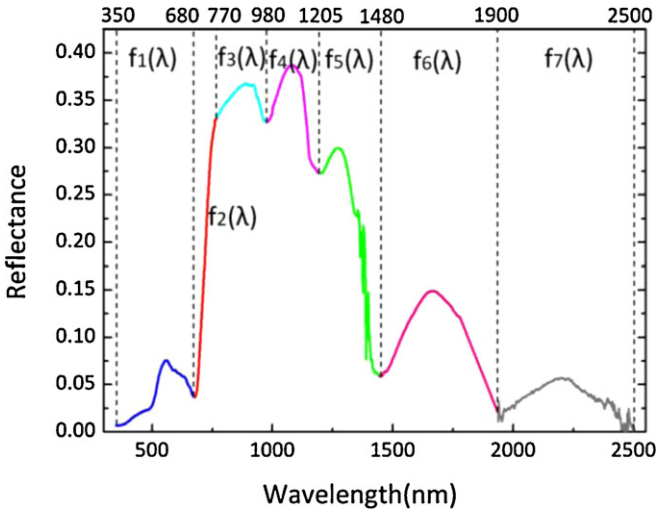

Fig. 3. Sketch map for piecewise function in the spectral curve.

system and UTM (Universal Transverse Mercator) projection system. The geometric error was less than 0.15 pixels. Then cubic convolution algorithm was used for brightness resampling.

3.2. Upscaling of input variables

3.2.1. Spectral data

A series of Hyperion reflectance were chose in pure pixel for rice, in addition, they kept the same geographical coordinates of ASD data collected (Fig. 1). For spectral resampling, ASD data is sampled at discrete wavelength positions at intervals of 10 nm to keep consistency with the Hyperion data in the spectral resolution. In order to improve the efficiency of scaling transformation in spectral data, it's important to find an effective way to diagnose or eliminate the outliers before retrieving and analyzing spectral information of satellite hyperspectral image. In this study, the regression analysis between Hyperion data and ASD data based on residual, which is larger than would be expected, at the 5% significance level, can be used to diagnose outliers (Chave and Thomson, 2003). The approach of elimination outliers has been recently used for upscaling biophysical variables such as LAI (leaf area index), and fAPAR (Fraction of Absorbed Photosynthetically Active Radiation) (Weiss et al., 2004). After diagnosing and eliminating outliers in Hyperion spectral data, the piecewise functions were developed to achieve scaling transformation of spectral data. The specific steps can be depicted as follows:

ASD data was depicted by seven piecewise functions according to the characteristic of shape in "peak and valley" (Fig. 3), they are computed by

$$y_A = \begin{cases} f_1(\lambda)\lambda \in (\lambda_0, \lambda_1) \\ f_2(\lambda)\lambda \in (\lambda_1, \lambda_2) \\ \vdots \\ f_r(\lambda)\lambda \in (\lambda_{r-1}, \lambda_r) \end{cases} \quad (1)$$

where y_A is the ASD reflectance, $f_r(\lambda)$ is the ASD reflectance value in the rth waveband region, r is the number of waveband region, $r = 1, 2, \ldots, 7$. The specific waveband range is described in the caption of Fig. 3.

Likely, the Hyperion data were depicted by seven piecewise functions, which are computed by

$$y_H = \begin{cases} g_1(\lambda)\lambda \in (\lambda_0, \lambda_1) \\ g_2(\lambda)\lambda \in (\lambda_1, \lambda_2) \\ \vdots \\ g_r(\lambda)\lambda \in (\lambda_{r-1}, \lambda_r) \end{cases} \quad (2)$$

where y_H is the Hyperion reflectance, $g_r(\lambda)$ is the Hyperion reflectance value in the rth waveband region, r is the number of waveband region, $r = 1, 2, \ldots, 7$.

$f_r(\lambda)$ and $g_r(\lambda)$ are canopy reflectance and pixel reflectance in different waveband region. The plant has very similar spectral response curves in different scales. More specifically, the shape in "peak and valley" is similar in the specific waveband range, regardless of canopy and pixel scale (Green et al., 1998). Therefore, it can be assumed that the same type of mathematic function exhibits in $f_r(\lambda)$ and $g_r(\lambda)$, spectral-response effect transformation of hyperspectral data to ASD data can be fulfilled by applying the scaling and translating of function, i.e.,

$$f_r(\lambda) = Ag_r(W\lambda + \theta) + K \quad (3)$$

where A and W are the scaling factors along vertical and horizontal axis, respectively; K and θ are the translating factors along vertical and horizontal axis, respectively.

As we know, the spectral reflectance value is a function of wavelength. In addition, the effective hyperspectral reflectance value ($f_r(\lambda)$ and $g_r(\lambda)$) in different remote sensors are both plotted at the corresponding effective wavelength positions (Zhao et al., 2010). That is to say, there is no need performing scaling and translating along horizontal axis. Thereby, in Eq. (3), $\theta = 0$, $W = 1$, the equation is simplified:

$$f_r(\lambda) = Ag_r(\lambda) + K \quad (4)$$

We can fulfill the scale transformation of hyperspectral data by directly applying Eq. (4), which belongs to piecewise functions. In fact, it can be considered that there is linear relationship for the transformation of spectral response effect in hyperspectral data to that of other scale. This agrees well with the previous study where the upscaling process is currently addressed by deriving an empirical transfer function that establishes a linear relationship between the field data to the corresponding satellite products (Zhao et al., 2010).

To evaluate the approximation accuracy, the fitting degree (F_D) between the transferred Hyperion reflectance and ASD data in the same wavelength region is calculated by

$$F_D = 1 - \frac{\sum_i^n (y_{HC} - y_A)^2}{\sum_{i=1}^n (y_{HC} - \overline{y_{HC}})^2} \quad (5)$$

where F_D is the fitting degree, y_A, y_{HC}, $\bar{y}_{HC}$ are the ASD reflectance, transferred Hyperion reflectance and average transferred Hyperion reflectance, respectively; n is the band number. F_D values range from 0 to 1. The higher F_D values, the better the performance of data transformation.

3.2.2. Soil data

In two study areas, soil sampling points (60 within Area A and 60 within Area B) were evenly distributed and chosen on the basis of 0.7 km × 0.7 km squares in each sample. For each sampling site, five replicate samples were collected, homogenized by hand mixing. As soil pH and OM are point data, ordinary kriging was used to interpolate from a single point to an area. Ordinary kriging provides an estimate at an unobserved location of a soil property data based on the weighted average of adjacent observed sites within a given

Table 1
The physical and chemical properties of the soils in Area A and Area B (mean + standard deviation).

Type	Study area	Total C (%)	Total N (%)	Total P (g/kg)	Total K (%)	Cu (mg/kg)	Zn (mg/kg)	Pb (mg/kg)	Cr (mg/kg)	As (mg/kg)	Cd (mg/kg)
Measured soil	A	0.18 + 0.06	1.90 + 0.76	0.60 + 0.08	1.39 + 0.21	56.35 + 6.47	50.38 + 4.98	18.95 + 7.45	14.12 + 4.49	9.27 + 1.89	0.36 + 0.01
	B	0.15 + 0.04	1.59 + 0.51	0.61 + 0.02	1.48 + 0.21	28.23 + 4.18	50.31 + 3.25	15.93 + 2.87	17.89 + 3.27	8.49 + 1.12	0.14 + 0.01
Background soil[a]		–	–	–	–	20.8	63.2	26.7	60.1	10.2	0.078

[a] Soil quality standard according to the Environment Monitoring Centre of China.

area. The method is usually applied in a case study for scaling-up in natural resources, ecological and environmental systems (Gertner et al., 2002; Wang et al., 2002; Triantafilis et al., 2004). The theory of ordinary kriging is derived from that of regionalized variables (Meul and Van Meirvenne, 2003; Lloyd and Atkinson, 2001; Atkinson and Lloyd, 2007). In this study, the pH and OM collected in the field were interpolated into 30 × 30 m grids by ordinary kriging to keep consistency with the Hyperion data in the spatial resolution. The spatial interpolation was conducted using the tool as Geostatistical Analyst in ArcGIS. The true prediction accuracy of ordinary kriging methods was evaluated by error mean (EM) and root mean square (RMS) (Li, 2010). They are computed by:

$$\mathrm{EM} = \frac{\sum_i^n [z(xi, yi) - z'(xi, yi)]}{n} \tag{6}$$

$$\mathrm{RMS} = \sqrt{\frac{\sum_i^n [z(xi, yi) - z'(xi, yi)]^2}{n}} \tag{7}$$

where n is the number of observations in the validation subset. $z(xi, yi)$ and $z'(xi, yi)$ are observations and predications in sampling coordinate (xi, yi). The lower EM and RMS indicate there is better prediction accuracy.

3.3. Establishment of model

3.3.1. Heavy metal assessment model at field-scale

The FHMA model for estimating heavy-metal concentrations in rice was established based on GDFNN by integrating spectral parameters and soil parameters. The GDFNN consists of an input layer, an output layer and several hidden layers, with the hidden layers belonging to the fuzzy interference system by carrying out fuzzy reasoning using the structure of neural network. The detail learning algorithm about GDFNN can be consulted in our pervious study (Liu et al., 2011b). Sensitive spectral parameters to heavy-metal contamination and soil parameters for influencing heavy-metal diffusion in rice were selected as input variables. We selected spectral parameters that have been introduced by Liu et al. (2011b). According to our investigation and analysis, the individual concentrations of Cu in rice served as output variables, and five parameters were taken as input variables, i.e., red edge position (REP), optimized soil adjusted vegetation index (OSAVI), normalized difference vegetation index (NDVI), organic matter (OM) and pH. When the individual concentrations of Cd in rice served as output variables, five parameters were also taken as input variables, i.e., difference vegetation index (DVI), OSAVI, NDVI, OM and pH. The calculation of above vegetation indices was displayed in Table 2. And it can be consulted in Liu et al. (2011b).

3.3.2. Heavy metal assessment model at regional-scale

The RHMA model was established based on the FHMA model, as discussed above. The procedure for the establishment of the RHMA model can be summarized as follows: (i) the input variables in regional-scale, which were consistent with those of the FHMA model, were obtained. The same input variables were considered in the FHMA and RHMA model. Here, it is noted that the spectral parameters of the RHMA and FHMA model had subtle difference in the selection of waveband, due to different spectral resolution in Hyperion data and ASD data. Detailed calculation for the spectral parameters was displayed in Table 2. (ii) These structure and rules of model, which had already been produced at a first stage (i.e., the training processing) in the development of the FHMA model, would be subsequently extracted. That is, once the FHMA model was established, the structure of the model was inherent. (iii) The RHMA model was established by aggregating input data (spectral parameters and soil parameters) based on the structure and rules extracted in order to predict heavy-metal concentrations in rice on regional-scale.

3.4. Assessment of model

To quantify performance of model for estimating heavy metal concentrations, four evaluation parameters between measured values and predicted values were calculated: model efficiency (ME), the correlation coefficient (R^2), root mean square error (RMSE) and mean absolute errors (MAE). The four parameters were computed by:

$$\mathrm{ME} = 1 - \frac{\sum_i^N (y_{ai} - y_{mi})^2}{\sum_{i=1}^N (y_{mi} - \bar{y}_m)^2} \tag{8}$$

$$R^2 = \frac{\left[\sum_{i=1}^N (y_{ai} - \bar{y}_a)\sum_{i=1}^N (y_{mi} - \bar{y}_m)\right]^2}{\sum_{i=1}^N (y_{ai} - \bar{y}_a)^2 \sum_{i=1}^N (y_{mi} - \bar{y}_m)} \tag{9}$$

$$\mathrm{RMSE} = \sqrt{\frac{\sum_{i=1}^N (y_{ai} - y_{mi})^2}{N - 1}} \tag{10}$$

Table 2
Spectral parameters used in ASD and Hyperion data.

Spectral parameters	Equation (ASD data)	Equation (Hyperion data)	Notation (Hyperion data)
REP	$D_{\lambda_i} = \frac{R(\lambda_{i+1}) - R(\lambda_{i-1})}{\lambda_{i+1} - \lambda_{i-1}}$, when D_{λ_i} is maximum value spectra between the red and NIR	$D_{\lambda_i} = \frac{R(\lambda_{i+1}) - R(\lambda_{i-1})}{\lambda_{i+1} - \lambda_{i-1}}$, when D_{λ_i} is maximum value spectra between the red and NIR	Between the red and NIR from 26th band to 34th band
OSAVI	$\frac{(1+0.5)(R_{800} - R_{670})}{(R_{800} + R_{670} + 0.5)}$	$\frac{(1+0.5)(R_{803} - R_{671})}{(R_{803} + R_{671} + 0.5)}$	803 nm and 671 nm for center wavelength of 38th and 25th band respectively
NDVI	$\frac{R_{760} - R_{695}}{R_{760} + R_{695}}$	$\frac{R_{762} - R_{691}}{R_{762} + R_{691}}$	762 nm and 691 nm for center wavelength of 34th and 27th band respectively
DVI	$R_{734} - R_{682}$	$R_{732} - R_{681}$	732 nm and 681 nm for center wavelength of 31st and 26th band respectively

R_i is the reflectance of band i.

$$\mathrm{MAE} = \frac{1}{N}\sum_{i=1}^{N}|y_{ai} - y_{mi}| \quad (11)$$

where y_{ai} and y_{mi} are the predicted value, measured value, $\bar{y}_a$ and $\bar{y}_m$ are the average predicted value and the average measured value, respectively. N is the sample number.

In the above four parameters, R^2 and ME were calculated to analyze the accuracy of predicted values versus measured values. R^2 and ME value range from 0 to 1. The higher the R^2 value is, the stronger the indication of an existing linear relationship between the measured and predicted values. Meanwhile, the higher ME values indicate prediction model's efficiency, whereas RMSE and MAE indicate estimation errors.

3.5. Analysis of spatial feature

In order to analyze of spatial feature of the heavy-metal concentrations in rice, the main procedures can be summarized as follows: (1) the different levels of heavy-metal pollution were distinguished. In this study, three stress levels of heavy-metal pollution were classified according to heavy-metal concentrations in rice (Liu et al., 2010), namely, safe level (<12 mg, for Cu; $<30\times10^{-3}$ mg, for Cd), pollution Level I (12–20 mg, for Cu; $30–60\times10^{-3}$ mg, for Cd), pollution Level II (>20 mg, for Cu; $>60\times10^{-3}$ mg, for Cd). The classification of stress levels was determined by below factors, including measured heavy-metal concentrations in rice under different pollution levels, China food health standards (GB 15199-94 and GBn238-84) and the ratio relationship of leaves and grains of heavy-metal concentrations in rice (Huang et al., 2009). (2) Heavy-metal concentrations in rice were displayed by using the two-dimensional map based on the image supervised classification mapping the distribution of rice. (3) The area and percentage of different levels of heavy-metal pollution were calculated and analyzed.

4. Results

4.1. Scale transformation of spectral data

4.1.1. Comparison between Hyperion and ASD data

A series of spectral reflectance from Hyperion image and ASD data were shown in Fig. 4(a). For clarity, Fig. 4(b) shows their respective mean value of spectral reflectance. As shown in Fig. 4(b), the shape of Hyperion reflectance in valley and peak in seven regions was similar to that of ASD data. The significant distinction was that the spectral curve of rice for Hyperion data was slightly higher than that of ASD data in the 450–680 nm and 770–2500 nm region. It was attributed to the differences between the spectral response functions of ASD and Hyperion, atmospheric correction, spatial heterogeneity, type of instrument and environmental conditions (canopy heterogeneity, illumination conditions) (Liu et al., 2006). All of which may lead to differences in the reflectivity at spaceborne or airborne hyperspectral imagery relative to the "true" reflectivity at ground hyperspectral data. Further investigation on this issue is needed.

Table 3
Fitting degree (F_D) and factors of scaling transformation for spectral data.

Spectral regions (nm)	K	A	F_D
350–680	−0.0077	0.6858	0.8125
680–770	−0.1119	1.4203	0.9335
770–980	+0.2087	0.3023	0.8789
980–1205	−0.0192	0.7998	0.9559
1205–1480	−0.1106	0.8762	0.9792
1480–1900	−0.0258	0.5253	0.9176
1900–2500	−0.1099	No	0.5366
350–2500			0.9861

4.1.2. Transformation result of Hyperion data

Based on the above discussion about the method of scale transformation for spectral data, transferred Hyperion data was shown in Fig. 4(c). It was observed that transferred Hyperion data has a close tendency to ASD data in terms of the fitting degree (F_D). The results of transformation in seven wavelength regions were summarized in Table 3. For translation factor (k), with the exception of the 770–980 nm region, the translation factor was taken down translation across y axis in the six other regions. For scaling factor (A), vertical scaling transform of spectral curve in the 660–770 nm region was stretched along y axis ($A>1$), while in the six other regions, vertical scaling transform of spectral curve was shortened along y axis ($A<1$). For fitting degree, there was low value ($F_D=0.5366$) in the 1900–2500 nm, it is because that they were influenced by the water vapor in atmosphere. While in the six other regions, F_D was greater than 0.8. Fortunately, we would obtain a good approximation ($F_D=0.9861$) between transferred Hyperion data and ASD data on the whole spectral curve. Therefore, it confirmed that the piecewise function is applicable to performing the scale transformation in spectral data.

4.1.3. Spatial distribution of spectral parameters from Hyperion data

For spectral parameters from Hyperion data, in seven wavelength regions, the respective piecewise function was established between ASD data ($f_r(\lambda)$) and Hyperion data ($g_r(\lambda)$). And then piecewise function was applied to Hyperion image in order to achieve upscaling of spectral data. The subtle differences were presented in the same spectral parameters in Areas A and B. Detailed statistics are presented in Table 4. The values of DVI, NDVI and OSAVI in Area B are higher than those in Area A. While the value of REP in Area B

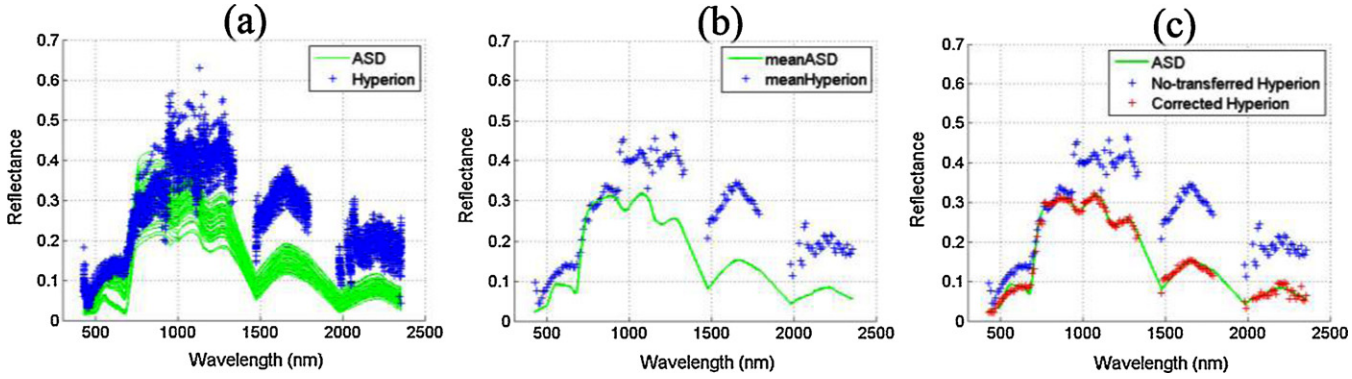

Fig. 4. Scale transformation of Hyperion data based on ASD data.

Table 4
Statistics of spectral input variables in Area A and Area B.

Study area	Input variables	Min	Max	Mean	Medium	Standard deviation
A	DVI	−0.17	0.56	0.07	0.06	0.06
	NDVI	−1.00	1.00	0.12	0.11	0.09
	OSAVI	−0.31	0.35	0.17	0.18	0.05
	REP (nm)	681	763	712	702	20
B	DVI	−0.07	0.61	0.13	0.12	0.05
	NDVI	−0.14	0.43	0.18	0.18	0.04
	OSAVI	0.02	0.35	0.21	0.21	0.03
	REP (nm)	681	742	701	691	17

is lower than that in Area A. The variation range of NDVI in Area B is greater than that in Area A. The standard deviation of four spectral parameters in Area A was higher than that in Area B.

4.2. Spatial interpolation of soil parameters

Ordinary kriging was applied for scaling-up spatial soil parameters across scales. Fig. 5 shows their spatial predictions for pH and OM in Area A and Area B. Detailed statistics are also presented in Table 5. The mean value of pH in Area B is lower than that in Area A, while the mean value of OM in Area B is greater than that in Area A. The standard deviation of two soil parameters in Area A is higher than that in Area B. For prediction accuracy, pH and OM in Area A and Area B had low EM and RMS values. It indicated that prediction accuracy of soil parameters by kriging interpolation methods got good performance. Additionally, whether pH or OM was being interpolated by ordinary kriging, the true prediction accuracy of Area B was better than those of Area A based on EM and RMS.

4.3. Heavy-metal concentrations in rice estimation

4.3.1. Field-scale model

Hyperion image data was acquired in maturity growth stage of rice. Therefore, in this study, data sets in the development of the FHMA model were obtained for different levels of heavy-metal pollution from the maturity growth stage of rice. In the FHMA model, the results are shown in Fig. 6, in which fuzzy rule, RMSE and actual output error change with more and more input variables entering the model. For Cu and Cd prediction, 10 fuzzy rules were both created. The R^2 values between the measured and predicted value were 0.9624 and 0.8329, respectively. Generally, regardless whether Cu or Cd was being estimated, FHMA model showed a satisfactory performance in model's efficiency and estimation errors. To detail, few fuzzy rule, low RMSE and high R^2 values were achieved with the FHMA model. In order to examine the credibility and stability of the FHMA model, the model was verified using testing sets based on the development of the network structure and fuzzy rules in the training stage. The relationship between the predicted and measured values of Cu and Cd concentration in rice leaves during the testing process is shown in Fig. 7. The constructed FHMA model (5 input variables, 10 fuzzy rules) provided a good fitting model for both of Cu and Cd concentration. R^2 between the measured and the predicated values were 0.8437 and 0.7112, respectively. Based on the above analysis, it concluded that the FHMA model has the good ability to estimate Cu and Cd concentrations in rice.

4.3.2. Regional-scale model

In order to estimate heavy-metal concentrations in rice on region scale, the RHMA model was constructed based on the development of the network structure and fuzzy rules in the FHMA model. Additionally, the input variables of the RHMA model are consistent with those of the FHMA model, including REP, OSAVI, NDVI, pH and OM that were used to predict concentrations of Cu in rice leaves. Likely, OSAVI, NDVI, DVI, pH and OM were taken as input variables to predict concentrations of Cd in rice leaves. The data sets of input variables were acquired by upscaling spatial data. Fig. 8(a) shows the spatial distribution of heavy-metal concentrations in rice leaves in Area A. Detailed statistics are presented in Table 6. For rice under Cd pollution, the area percentage of rice under safe level, pollution Level I and pollution Level II were 29.78%, 51.67% and 18.73% of the total rice area in Area A, respectively; While for rice under Cu pollution, the area percentage of rice under safe level, pollution

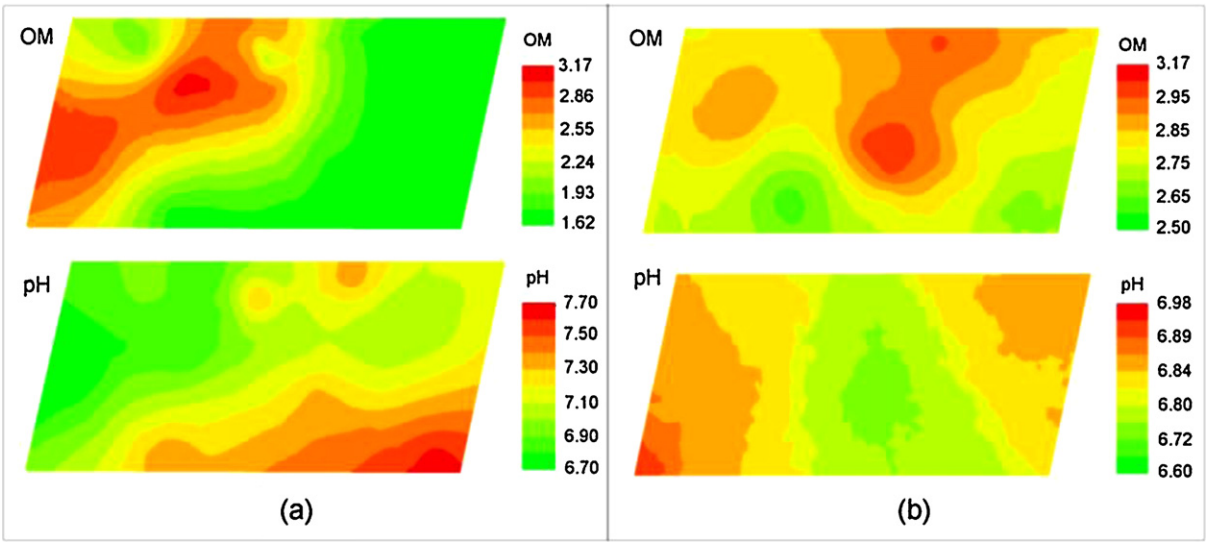

Fig. 5. Predicted value of pH and OM in study areas using ordinary kriging method (a) Area A and (b) Area B.

Table 5
Statistics of soil input variables in Area A and Area B.

Study area	Input variables	Min	Max	Mean	Medium	Standard deviation	Predication accuracy	
							EM (10^{-2})	RMS
A	pH	6.69	7.38	7.05	7.08	0.17	1.66	0.17
	OM	2.00	2.79	2.31	2.23	0.23	2.57	0.34
B	pH	6.76	6.89	6.83	6.84	0.03	0.26	0.09
	OM	2.74	2.96	2.85	2.84	0.05	0.64	0.12

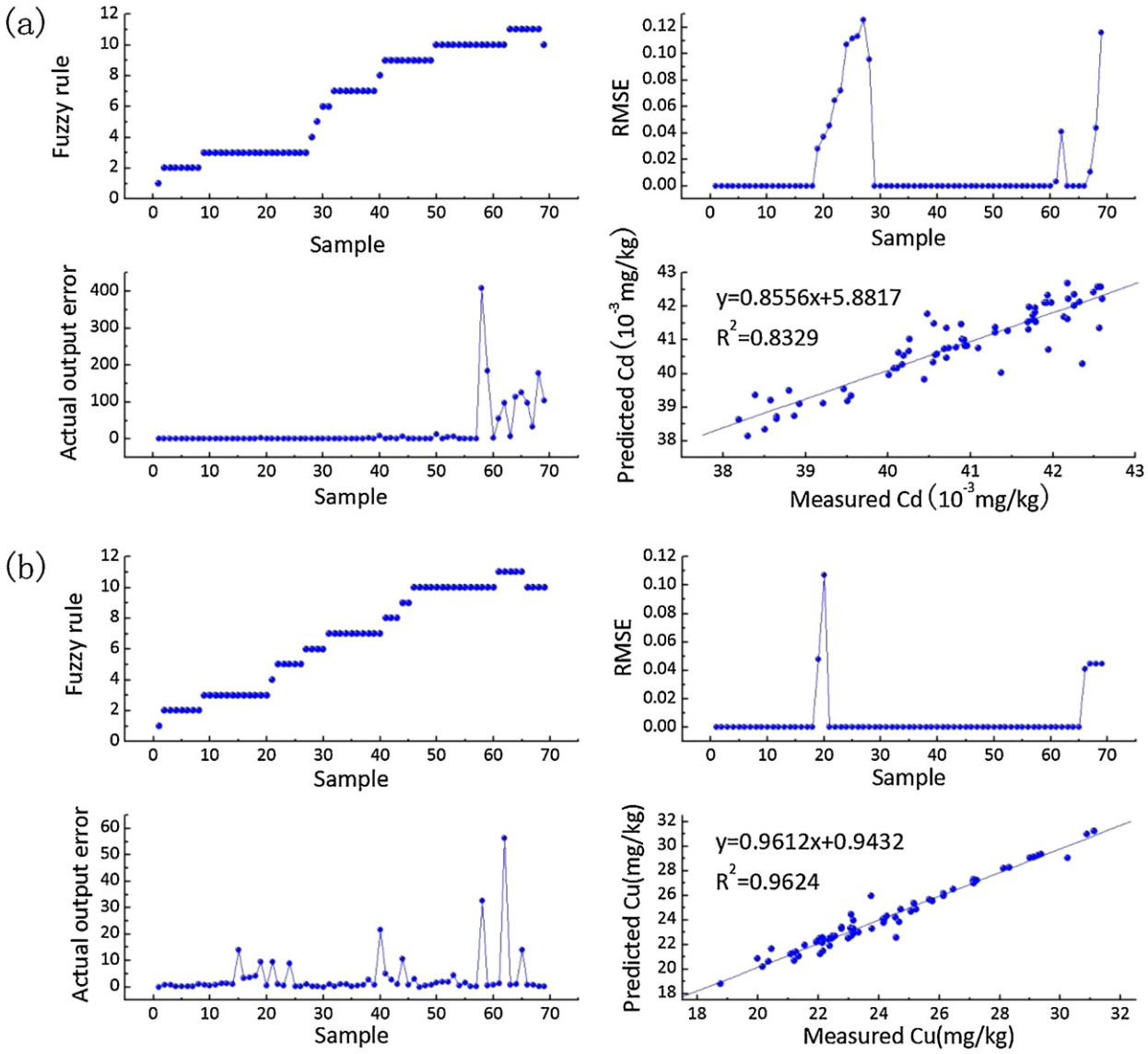

Fig. 6. Dynamic results of the field-scale spectral analysis and assessment model for estimating (a) Cd concentration and (b) Cu concentration.

Table 6
Statistics of Cu and Cd concentration in rice leaves in Area A and Area B.

Study area	Heavy metal	Safe level		Level I		Level II		Total rice area (10^2 m^2)
		Area (10^2 m^2)	Percentage (%)	Area (10^2 m^2)	Percentage (%)	Area (10^2 m^2)	Percentage (%)	
A	Cu	3006	12.10	15,903	64.02	5931	23.88	24,840
	Cd	7398	29.78	12,834	51.67	4653	18.73	
B	Cu	88,029	58.51	50,076	33.29	12,339	8.20	150,444
	Cd	97,515	64.82	42,714	28.39	10,215	6.79	

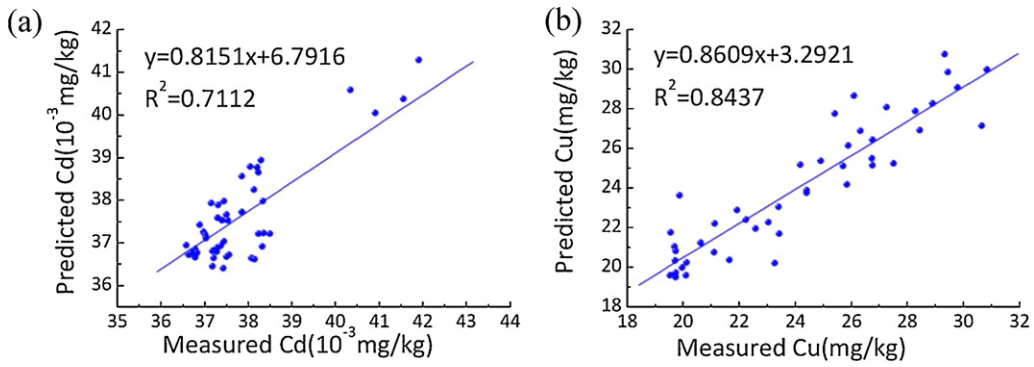

Fig. 7. Comparison of the predicted and measured in FHMA model (a) Cd and (b) Cu concentration in rice leaves.

Level I and pollution Level II were 12.10%, 64.02% and 23.88% of the total rice area in Area A, respectively. On the whole, regardless whether Cu or Cd was being estimated, the most of rice were suffered by the pollution Level I, while the small part of rice was at safe level in Area A. It was attributed to the rice planted nearby to the center of the city of Changchun. It was in good agreement with the actual distribution of heavy-metal concentration in paddy. This study reveals that the RHMA model established can be used for predicting heavy-metal concentrations in rice.

4.3.3. Validation of regional-scale model

To illustrate the ability of the RHMA model to be used extensively, we apply it to another study area (i.e., Area B). During the validation of the RHMA model, the input variables of model were again REP, OSAVI, NDVI, pH and OM to predict concentrations of Cu in rice leaves. Likely, OSAVI, NDVI, DVI, pH and OM were taken as input variables to predict concentrations of Cd in rice leaves. The data sets of input variables were obtained by performing the upscaling transformation of spectral parameters and soil parameters. Fig. 8(b) shows the result of prediction and the spatial distribution of heavy-metal concentrations in rice leaves. Detailed statistics are also presented in Table 6. For rice under Cd pollution, the area percentage of rice under safe level, pollution Level I and pollution Level II were 64.82%, 28.39% and 6.79% of the total rice area in Area B, respectively; While for rice under Cu pollution, the area percentage of rice under safe level, pollution Level I and pollution Level II were 58.51%, 33.29% and 8.20% of the total rice area in Area B, respectively; Generally, regardless of Cd or Cu, the minority of rice was suffered by the heavy-metal stress, the majority of rice was at safe level. In addition, the highest area percentage of rice under Cd or Cu pollution in the total rice area were measured at safe level, followed by pollution Level I, then pollution Level II in Area B.

Further, to examine the credibility and stability of RHMA, the model was verified using 20 data sets, which derived from field measurement in Area B. Fig. 9 shows the plots between measured and model predicted values of Cd and Cu concentration in rice leaves. The constructed RHMA provided a good fitting model for both of Cd and Cu. The R^2 values for the Cd and Cu were 0.7704 and 0.8407, respectively. More detailed performance parameters for the model for estimating of Cu and Cd concentration of rice leaves were calculated in Table 7. As seen in Table 7, while predicting both Cd and Cu concentrations, R^2 and ME were both above 0.70. Here, the RMSE values were 15.02 and 2.83 for Cd and Cu, respectively; the MAE values were 51.64 and 21.10 for Cd and Cu, respectively. Compared with Cu concentration, Cd concentration had greater estimation error with higher RMSE and MAE. Furthermore, to quantify difference in model's performance between RHMA model and FHMA model for estimating heavy metal concentrations, performance

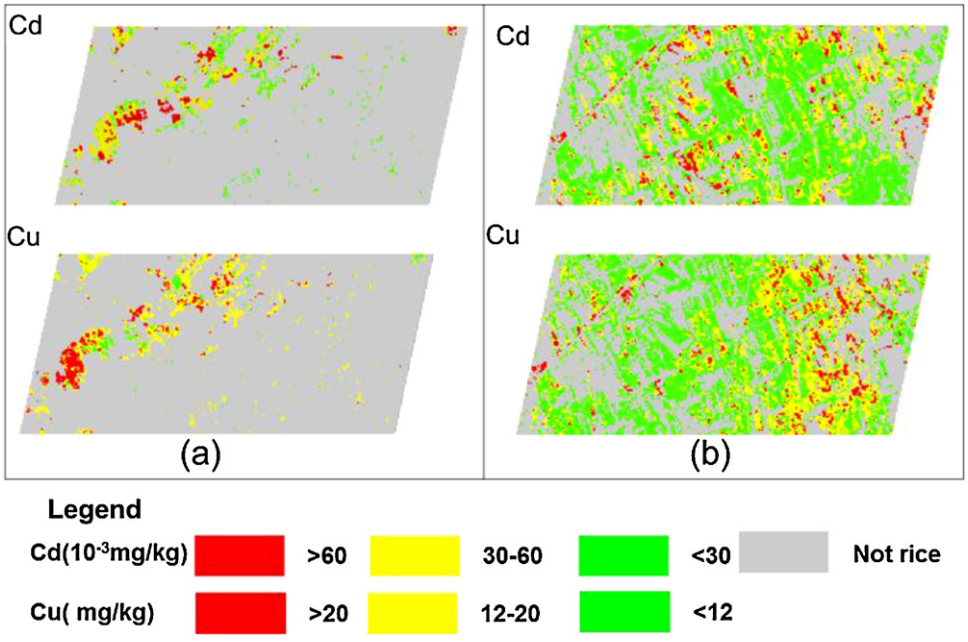

Fig. 8. Spatial distribution of heavy-metal concentrations in rice using the RHMA model in areas (a) Area A and (b) Area B.

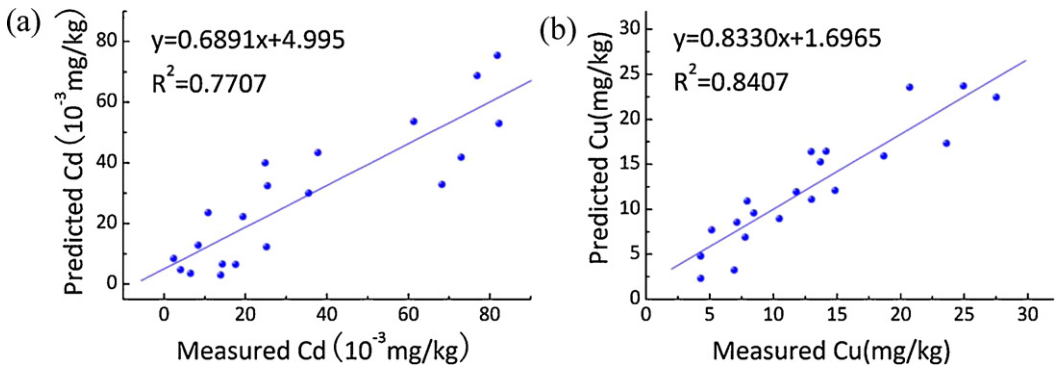

Fig. 9. Comparison of the predicted and measured in RHMA model (a) Cd and (b) Cu concentration in rice leaves.

Table 7
Comparison of model's performance between FHMA and RHMA model for estimating of Cu and Cd concentration in rice leaves.

Model	Heavy metal	ME	R^2	RMSE	MAE
FHMA	Cd	0.67	0.7112	0.69	1.45
	Cu	0.84	0.8437	1.40	4.36
RHMA	Cd	0.72	0.7707	15.02	51.64
	Cu	0.84	0.8407	2.83	21.10

parameters for the FHMA model were also displayed in Table 7. From Table 7, RHMA and FHMA model had good performance in the accuracy of model predictions with having similar R^2 and ME. It implied that it was effective to estimate regional heavy metal concentrations in rice by upscaling of FHMA model. However, estimation errors of RHMA model were greater than those of FHMA model.

5. Discussion

It is essential for agricultural production, food security, and the human habitat to use remote sensing technology to provide large-scale information about the precise levels of heavy metal stress. However, it is difficult to assess stress levels of crops with heavy metal pollution on a large scale using spaceborne or airborne images directly. The primary reason is that various environment-induced noise in the spaceborne or airborne images masks subtle features associated with stress (Collins et al., 1983). Some research has been undertaken to establish a relationship between heavy metal concentrations in crops and ground hyperspectral reflectance characteristics in both controlled laboratory conditions and field conditions (Chi et al., 2009; Liu et al., 2010, 2011a). Significant progress has been made in field-scale heavy metal estimation in crops. Therefore, in this study, we propose the novel idea for estimating regional heavy metal concentrations in crop by scaling the FHMA model up based on our previous study (Liu et al., 2011b). Near surface remote sensing as a technique to monitor heavy metal pollution in crop has two merits in order to extrapolate the results regionally. First, biochemical data of crops under heavy metal stress were taken almost simultaneously with measurements of canopy spectral reflectance. In contrast, it is difficult to keep the acquired airborne hyperspectral imagery synchronization with measurements of the biochemical data of the crop under heavy metal stress. Second, it is convenient to obtain a number of crop reflectance spectra data using proximal sensing in a field scale in order to explore the relationship between spectra and metal concentrations.

Whether estimation of regional heavy metal concentrations in crop is accurate or not depends on the strategy scaling the FHMA model up. In fact, many researchers have developed effective methods, such as wavelet transform (White et al., 2005; Biswas and Si, 2011), hierarachical theory (Wu and David, 2002; Zhang and Arhonditsis, 2009), geostatistical methods (Kok and Veldkamp, 2001; Van de Giesen et al., 2011), in order to deal with upscaling problems pertaining to hydrology, ecology, geography, water resources management and agricultural systems.

Our present study focuses on scaling the input variables of the FHMA model up, rather than adjusting the model structure or re-establishing a new model. It is because the FHMA model is based on the link mechanism of soil heavy metal contamination, heavy metal accumulation in crops and heavy metal-induced spectral response. Mechanism of crop heavy metal assessment model is similar whether they occur in the finer scale or in the coarser scale. In addition, different upscaling methods have been considered when dealing with different types of input variables. For spectral reflectance, the significant difference was observed between Hyperion data and ASD data (Fig. 4). In nature, it was demonstrated that there is a difference between spectral reflectance of the canopy and the spectral reflectance of a pixel. Some researchers applied piecewise regression model to solve non-linear problems in different spatial resolution data (Kustas et al., 2003; Jeganathan et al., 2011). Here, piecewise function was used to correct Hyperion reflectance to ASD reflectance according to the shape of the reflectance spectrum, which made Hyperion reflectance into "true" reflectance in ground hyperspectral data in order to reduce estimation errors induced by spectral parameters. Seven piecewise functions were used based on the shape of "peak" and "valley" in plant reflectance. Going into further detail, "green peak" in visible bands "red edge" in near infrared bands and other five "peak" between water absorption center of plant reflectance about 960 nm, 1100 nm in near infrared bands, and 1400 nm, 1900 nm and 2700 in short-wave infrared bands (Gerstl and Zardecki, 1985; Hurcom et al., 1996). In addition, our result showed that it is effective to perform spectral scale transformation by cutting seven piecewise functions. While for soil parameters, their regional parameters were obtained by ordinary kriging interpolation, which is widely used in agriculture, ecology and environmental systems (Gertner et al., 2002; Wang et al., 2002; Triantafilis et al., 2004). It suggested that different approaches to upscaling should be taken into consideration to deal with different types of variables. It is feasible to estimate regional heavy-metal concentrations in rice by scaling the FHMA model up. Additionally, the established model can be successfully applied to two different study areas (i.e., Area A and Area B). It concluded that the RHMA model is reproductive and is used extensively under different environmental conditions by combining soil parameters with spectral parameters. Our previous study has also demonstrated that such model is universal and transferable (Liu et al., 2011b). The major reason is that FHMA model based on GDFNN algorithm, the algorithm itself possesses the advantages of strong self-study ability, information fusion and fuzzy reasoning (Er et al., 2004; Wen and Zhu, 2004). And also because the involvement

of soil parameters as input variables facilitates the application of FHMA model in different soil environmental conditions and thus increases the ability of model to be used extensively.

In this research, in order to provide regional-scale information about levels of heavy metal pollution, the upscaling method of a field-scale heavy metal assessment model was proposed. This approach may offer insight into monitoring various environments on a large scale, such as agro-ecosystems and the water environment.

6. Conclusions

In this study, we have presented a method for estimating regional heavy metal concentrations in crop. The preliminary FHMA model was created to estimate field-scale heavy-metal concentrations in rice based on the GDFNN algorithm by integrating spectral parameters, which derived from the field measurement ASD data, and soil parameters. Five parameters (for Cu, REP, OSAVI, NDVI, OM, and pH; for Cd, DVI, OSAVI, NDVI, OM and pH) were taken into consideration as input variables of the FHMA model. The results showed that in the FHMA model for estimating Cu during training and testing stages, the R^2 value between the measured and the predicted value were over 0.80. While the FHMA model was used for estimating Cd during training and testing stages, the R^2 value was greater than 0.75. Fuzzy rules were both 10, regardless whether Cu or Cd was being estimated. It demonstrated that the FHMA model has both a high level of accuracy as well as a compact network structure.

This study focuses on upscaling issues referring to the transfer of heavy-metal assessment model. The final results showed that the RHMA model performed well in assessing the stress levels of rice under heavy-metal pollution with R^2 and ME over 0.70. Further, the RHMA model established was verified by applying it to another study area. Fortunately, the predicted results were both in good agreement with the actual distribution of heavy-metal concentration in rice. It confirmed that the RHMA model is efficient and universally applicable to estimating heavy-metal concentrations in rice on regional-scale. This study suggested that the piecewise function is promising for transferring of spectral data from one scale to another.

In conclusion, the RHMA model can successfully estimate heavy-metal concentrations in rice at regional scale by upscaling of FHMA model.

Conflict of interest

The authors declare that they have no competing interests.

Acknowledgements

This research was supported by the National Natural Science Foundation of China (no. 40771155) and the National High-Tech R&D Program of China (no. 2007AA12Z174). The authors wish to thank the anonymous reviewers for their constructive comments that helped improve the scholarly quality of the paper.

References

Adam, M., Van Bussel, L.G.J., Leffelaar, P.A., Van Keulen, H., Ewert, F., 2011. Effects of modelling detail on simulated potential crop yields under a wide range of climatic conditions. Ecological Modelling 222 (1), 131–143.

Atkinson, P.M., Lloyd, C.D., 2007. Non-stationary variogram models for geostatistical sampling optimisation: an empirical investigation using elevation data. Computers & Geosciences 33 (10), 1285–1300.

Bao, S.D., 2005. Soil Analytical Methods of Agronomic Chemistry. China Agricultural Science and Technology Press, Beijing, pp. 66–82 (in Chinese).

Becker, A., Braun, P., 1999. Disaggregation, aggregation and spatial scaling in hydrological modeling. Journal of Hydrology 217 (3), 239–252.

Biswas, A., Si, B.C., 2011. Application of continuous wavelet transform in examining soil spatial variation: a review. Mathematical Geosciences 43 (3), 379–396.

Chave, A.D., Thomson, D.J., 2003. A bounded influence regression estimator based on the statistics of the hat matrix. Journal of the Royal Statistical Society Series C: Applied Statistics 52, 307–322.

Chi, G.Y., Chen, X., Shi, Y., Liu, X.H., 2009. Spectral response of rice (*Oryza sativa* L.) leaves to Fe^{2+} stress. Science in China Series C: Life Sciences 52 (8), 747–753.

Clevers, J., Kooistra, L., Salas, E.A.L., 2004. Study of heavy metal contamination in river floodplains using the red-edge position in spectroscopic data. International Journal of Remote Sensing 25 (19), 3883–3895.

Collins, W., Chang, S.H., Raines, G., Canney, F., Ashley, R., 1983. Airborne biogeophysical mapping of hidden mineral-deposits. Economic Geology 78 (4), 737–749.

Datt, B., McVicar, T.R., Van Niel, T.G., Jupp, D.L.B., Pearlman, J.S., 2003. Preprocessing EO-1 Hyperion hyperspectral data to support the application of agricultural indexes. IEEE Transactions on Geoscience and Remote Sensing 41 (6), 1246–1259.

Er, M.J., Tan, T.P., Loh, S.Y., 2004. Control of a mobile robot using generalized dynamic fuzzy neural networks. Microprocessors and Microsystems 28 (9), 491–498.

Ewert, F., van Ittersum, M.K., Heckelei, T., Therond, O., Bezlepkina, I., Andersen, E., 2011. Scale changes and model linking methods for integrated assessment of agri-environmental systems. Agriculture, Ecosystems & Environment 142 (1–2), 6–17.

Font, R., Del Río, M., De Haro, A., 2002. Use of near infrared spectroscopy to evaluate heavy metal content in *Brassica juncea* cultivated on the polluted soils of the Guadiamar River area. Fresenius Environmental Bulletin 11 (10), 777–781.

Font, R., Del Rio, M., Velez, D., Montoro, R., De Haro, A., 2004. Use of near-infrared spectroscopy for determining the total arsenic content in prostrate amaranth? Science of the Total Environment 327 (1–3), 93–104.

Gerstl, S.A.W., Zardecki, A., 1985. Coupled atmosphere/canopy model for remote sensing of plant reflectance features. Applied Optics 24 (1), 94–103.

Gertner, G., Wang, G.X., Fang, S.F., Anderson, A.B., 2002. Mapping and uncertainty of predictions based on multiple primary variables from joint co-simulation with Landsat TM image and polynomial regression. Remote Sensing of Environment 83 (3), 498–510.

Green, R.O., Eastwood, M.L., Sarture, C.M., Chrien, T.G., Aronsson, M., Chippendale, B.J., Faust, J.A., Pavri, B.E., Chovit, C.J., Solis, M.S., Olah, M.R., Williams, O., 1998. Imaging spectroscopy and the Airborne Visible Infrared Imaging Spectrometer (AVIRIS). Remote Sensing of Environment 65 (3), 227–248.

Hong, S.H., Hendrickx, J.M.H., Borchers, B., 2009. Upscaling of SEBAL derived evapotranspiration maps from Landsat (30 m) to MODIS (250 m) scale. Journal of Hydrology 370 (1–4), 122–138.

Hong, S.H., Hendrickx, J.M.H., Borchers, B., 2005. Effect of scaling transfer between evapotranspiration maps derived from LandSat 7 and MODIS images. In: Targets and Backgrounds XI: Characterization and Representation, pp. 147–158.

Huang, Y.Z., Hu, Y., Liu, Y.X., 2009. Combined toxicity of copper and cadmium to six rice genotypes (*Oryza sativa* L.). Journal of Environmental Sciences 21 (5), 647–653.

Hurcom, S.J., Harrison, A.R., Tabcuerner, M., 1996. Assessment of biophysical vegetation properties through spectral decomposition techniques. Remote Sensing of Environment 56 (3), 203–214.

Jeganathan, C., Hamm, N.A.S., Mukherjee, S., Atkinson, P.M., Raju, P.L.N., Dadhwal, V.K., 2011. Evaluating a thermal image sharpening model over a mixed agricultural landscape in India. International Journal of Applied Earth Observation and Geoinformation 13 (2), 178–191.

Keshava, N., 2001. Best bands selection for detection in hyperspectral processing. IEEE International Conference on Acoustics, Speech, and Signal Processing, 3149–3152.

Keshava, N., 2003. Angle-based band selection for material identification in hyperspectral processing. In: Shen, Sylvia S., Lewis, Paul E. (Eds.), Algorithms and Technologies for Multispectral, Hyperspectral and Ultraspectral Imagery IX, Proceedings of the SPIE, vol. 5093. , pp. 440–451.

Kok, K., Veldkamp, A., 2001. Evaluating impact of spatial scales on land use pattern analysis in Central America. Agriculture Ecosystems & Environment 85 (1–3), 205–221.

Kooistra, L., Salas, E.A.L., Clevers, J., Wehrens, R., Leuven, R., Nienhuis, P.H., Buydens, L.M.C., 2004. Exploring field vegetation reflectance as an indicator of soil contamination in river floodplains. Environmental Pollution 127 (2), 281–290.

Kooistra, L., Wehrens, R., Leuven, R., Buydens, L.M.C., 2001. Possibilities of visible-near-infrared spectroscopy for the assessment of soil contamination in river floodplains. Analytica Chimica Acta 446 (1–2), 97–105.

Kustas, W.P., Norman, J.M., Anderson, M.C., French, A.N., 2003. Estimating sub-pixel surface temperatures and energy fluxes from the vegetation index-radiometric temperature relationship. Remote Sensing of Environment 85, 429–440.

Li, Y., 2010. Can the spatial prediction of soil organic matter contents at various sampling scales be improved by using regression kriging with auxiliary information? Geoderma 159 (1–2), 63–75.

Liu, M.L., Liu, X.N., Ding, W.C., Wu, L., 2011a. Monitoring stress levels on rice with heavy metal pollution from hyperspectral reflectance data using wavelet-fractal analysis. International Journal of Applied Earth Observation and Geoinformation 13 (2), 246–255.

Liu, M.L., Liu, X.N., Wu, M.X., Li, L.F., Xiu, L.N., 2011b. Integrating spectral indices with environmental parameters for estimating heavy metal concentrations in rice using dynamic fuzzy neural-network model. Computers & Geosciences 37 (10), 1642–1652.

Liu, M.L., Liu, X.N., Li, M., Fang, M.H., Chi, W.X., 2010. Neural-network model for estimating leaf chlorophyll concentration in rice under stress from heavy metals using four spectral indices. Biosystems Engineering 106 (3), 223–233.
Liu, Y.B., Hiyama, T., Yamaguchi, Y., 2006. Scaling of land surface temperature using satellite data: a case examination on ASTER and MODIS products over a heterogeneous terrain area. Remote Sensing of Environment 105 (2), 115–128.
Lloyd, C.D., Atkinson, P.M., 2001. Assessing uncertainty in estimates with ordinary and indicator kriging. Computers & Geosciences 27 (8), 929–937.
Martinez, B., Garcia-Haro, F.J., Camacho-de Coca, F., 2009. Derivation of high-resolution leaf area index maps in support of validation activities: application to the cropland Barrax site. Agricultural and Forest Meteorology 149 (1), 130–145.
Meul, M., Van Meirvenne, M., 2003. Kriging soil texture under different types of nonstationarity. Geoderma 112 (3–4), 217–233.
Nagarajan, K., Krekeler, C., Slatton, K.C., Graham, W.D., 2010. A scalable approach to fusing spatiotemporal data to estimate streamflow via a Bayesian network. IEEE Transactions on Geoscience and Remote Sensing 48 (10), 3720–3732.
Noomen, M.F., Skidmore, A.K., van der Meer, F.D., Prins, H.H.T., 2006. Continuum removed band depth analysis for detecting the effects of natural gas, methane and ethane on maize reflectance. Remote Sensing of Environment 105 (3), 262–270.
Noomen, M.F., van der Werff, H.M.A., van der Meer, F.D., 2012. Spectral and spatial indicators of botanical changes caused by long-term hydrocarbon seepage. Ecological Informatics 8, 55–64.
Parry, M.L., Rosenzweig, C., Iglesias, A., Livermore, M., Fischer, G., 2004. Effects of climate change on global food production under SRES emissions and socio-economic scenarios. Global Environmental Change 14 (1), 53–67.
Pelosi, C., Goulard, M., Balent, G., 2010. The spatial scale mismatch between ecological processes and agricultural management: do difficulties come from underlying theoretical frameworks? Agriculture, Ecosystems & Environment 139 (4), 455–462.
Petrosillo, I., Zaccarelli, N., Zurlini, G., 2010. Multi-scale vulnerability of natural capital in a panarchy of social–ecological landscapes. Ecological Complexity 7 (3), 359–367.
Rosso, P.H., Pushnik, J.C., Lay, M., Ustin, S.L., 2005. Reflectance properties and physiological responses of *Salicornia virginica* to heavy metal and petroleum contamination. Environmental Pollution 137 (2), 241–252.
Schroder, W., Schmidt, G., 2006. A methodological approach of site selection and data analysis to provide model input data for an up-scaling of population effects of transgenetic oilseed rape in Northern Germany. Ecological Indicators 6 (1), 168–183.
Triantafilis, J., Odeh, I.O.A., Warr, B., Ahmed, M.F., 2004. Mapping of salinity risk in the lower Namoi valley using non-linear kriging methods. Agricultural Water Management 69 (3), 203–229.
Van de Giesen, N., Stomph, T.-J., Ajayi, A.E., Bagayoko, F., 2011. Scale effects in Hortonian surface runoff on agricultural slopes in West Africa: field data and models. Agriculture Ecosystems & Environment 142 (1–2), 95–101.
Volk, M., Hirschfeld, J., Dehnhardt, A., Schmidt, G., Bohn, C., Liersch, S., Gassman, P.W., 2008. Integrated ecological-economic modelling of water pollution abatement management options in the Upper Ems River Basin. Ecological Economics 66 (1), 66–76.
Wang, G., Wente, S., Gertner, G.Z., Anderson, A., 2002. Improvement in mapping vegetation cover factor for the universal soil loss equation by geostatistical methods with Landsat Thematic Mapper images. International Journal of Remote Sensing 23 (18), 3649–3667.
Weiss, M., Baret, F., Smith, G.J., Jonckheere, I., Coppin, P., 2004. Review of methods for in situ leaf area index (LAI) determination: part II. Estimation of LAI, errors and sampling. Agricultural and Forest Meteorology 121 (1–2), 37–53.
Wen, S.H., Zhu, Q.G., 2004. Generalized dynamic fuzzy neural network-based tracking control of robot manipulators. In: IEEE Proceedings of the 2004 International Conference on Machine Learning and Cybernetics, vols. 1–7, New York, pp. 812–816.
White, M.A., Schmidt, J.C., Topping, D.J., 2005. Application of wavelet analysis for monitoring the hydrologic effects of dam operation: Glen Canyon Dam and the Colorado River at Lees Ferry, Arizona. River Research and Applications 21 (5), 551–565.
Wu, J.G., David, J.L., 2002. A spatially explicit hierarchical approach to modeling complex ecological systems: theory and applications. Ecological Modelling 153 (1–2), 7–26.
Zarco-Tejada, P.J., Miller, J.R., Noland, T.L., Mohammed, G.H., Sampson, P.H., 2001. Scaling-up and model inversion methods with narrow-band optical indices for chlorophyll content estimation in closed forest canopies with hyperspectral data. IEEE Transactions on Geoscience and Remote Sensing 39 (7), 1491–1507.
Zengin, F.K., Munzuroglu, O., 2005. Effects of some heavy metals on content of chlorophyll, proline and some antioxidant chemicals in bean (*Phaseolus vulgaris* L.) seedlings. Acta Biologica Cracoviensia Series Botanica 47 (2), 157–164.
Zhang, W., Arhonditsis, G.B., 2009. A Bayesian hierarchical framework for calibrating aquatic biogeochemical models. Ecological Modelling 220 (18), 2142–2161.
Zhao, H.J., Jia, G.R., Li, N., 2010. Transformation from hyperspectral radiance data to data of other sensors based on spectral superresolution. IEEE Transactions on Geoscience and Remote Sensing 48 (11), 3903–3912.
Zobeck, T.M., Parker, N.C., Haskell, S., Guoding, K., 2000. Scaling up from field to region for wind erosion prediction using a field-scale wind erosion model and GIS. Agriculture, Ecosystems & Environment 82 (1–3), 247–259.